UTILIZING OF ELLIPTIC DOMAIN OF INFLUENCE FORMULATION OF MESHFREE METHOD FOR SOLVING OF LEFM PROBLEMS

Haider Khazal Mehbes **Dr.Ameen Ahmad Nassar** **Hassanein Ibraheem Khalaf**

Rafid Jabbar Mohammed

Mechanical Engineering Department

College of Engineering

University of Basrah

Basrah / Iraq

ABSTRACT

This paper presents an efficient meshless method by using an elliptic domain rather than traditional isotropic domain of influence. The method involves an element free Galerkin formulation in conjunction with an anisotropic weight function. In the elliptic weight function, each node has three characteristic indications that are major radius, inner radius, and the direction of the local domain. Furthermore, the space that will be covered by the elliptic will be less than the area of the circle (isotropic) at the same main diameter. This means leaving many points of integration are not necessary. Therefore, the computational cost was decreased. For the first time, the elliptic domain is used in the problems of linear elastic fracture mechanism LEFM. MATLAB codes are used in obtaining the results of this research. The results are compared with those present in the literature.

Keywords: Meshless Methods, Element Free Galerkin Method, Elliptic Domain of Influence

فوائد تشكيل المجال البيضوي في الطريقة اللاشبكية لحل مشاكل الكسر المرن الخطي

مدرس مساعد حيدر خزعل محبس **أستاذ مساعد دكتور امين احمد نصار** **مدرس مساعد حسنين ابراهيم خلف**

مدرس مساعد رافد جبار محمد

قسم الهندسة الميكانيكية

كلية الهندسة

جامعة البصرة

البصرة – العراق

الملخص

يعرض هذا البحث طريقة لاشبكية كفؤه باستخدام المجال البيضوي (elliptic domain) بدلا من المجال المتماثل الخواص التقليدي(circular domain). الطريقة تتضمن تشكيل الطريقة اللاشبكية EFG مع داله اختبار غير متماثلة الخواص. في داله الاختبار البيضوي، كل عقدة (node) لها ثلاثة بيانات مميزة هي نصف قطر رئيسي المركز هو العقدة، نصف قطر ثانوي، واتجاه المجال الموضعي. علاوة على ذلك، الفضاء الذي سيغطى بواسطة البيضوي سيكون اقل من المجال الدائري (isotropic) وبنفس القطر الرئيسي. وهذا يعني ترك الكثير من نقاط التكامل الغير ضرورية. وبذلك ، وقت التحليل

(computational cost) ينخفض. للمرة الأولى ، المجال البيضوي يستعمل في مسائل الية الكسر المرنة الخطية LEFM. تم استخدام برنامج ماتلاب في استحصال نتائج هذا البحث.مقارنة النتائج مع بحوث مماثلة تم للتحقق من كفاءة المجال البيضوي.

INTRODUCTION

In the recent year, a kind of meshless or meshfree method has been developed based on moving least square (MLS) approximation [1], which does not require a structured mesh or elements. Among these methods, element free Galerkin method (EFGM) [2-5] is particularly attractive, due to its uncomplicatedness, easing of numerical difficulties of mesh entanglement, faster rate of convergence, and a formulation that corresponds to well-established FEM. Because of the MLS properties in the continuity, and the smooth approximation results, EFGM use to extract the data in the discontinuities such as in the crack [6-10], and shear band [11-14].

One of the drawbacks of EFGM is forced imposition of essential boundary conditions rather than the direct method. This is existed because of the MLS does not have the Kronecker delta property, where the shape function associated with a node is not exactly equal to one at this node, and this shape function is not exactly zero at the other nodes in the domain. This drawback is solved by using a variety of the enforced boundary methods [4, 15, 16].

In the MLS approximation, each node has a domain of influence, in which a function of compact support is used as a weight function. The weight function determines the intensity of the effect of a node at various points in its domain of influence. Figure 1 represents discretization using meshless methods: nodes, circular domains of influence. Examples of commonly used test functions are exponential function, and spline functions. Excellent details on systematic ways to construct weigh functions can be found in [15, 17-18].

The nodal influence domain is usually considered having a consolidated form in the shape of a circle or sphere. In the EFGM, accuracy and effectiveness are dependent on the nodal domain of influence and type of the weight function. In this work, non-consolidated (anisotropic) weight function in the elliptic form is introduced to improve the efficiency of the EFGM in some problems. In the using non-consolidated weight functions, the influence domain of each node may vary with direction. As a consequence, the definition of the influence domain based on non-consolidated weight function, improves the numerical efficiency of EFGM. In such case, the influence domain of each node can be determined so that the nodal overlapping decreases. Thus, good results can be achieved with less computational efforts.

MILS APPROXIMATION

It has been shown that moving least-square methods and weight functions share many features for the constructing the approximation of the solution. In the MLS technique that presented by [1], the approximation $\boldsymbol{u^h(x)}$ is expressed as the inner product of a vector of the polynomial basis $\mathbf{P}(\boldsymbol{x})$ and a vector of the coefficient $\mathbf{a}(\boldsymbol{x})$.

$$u^h(\boldsymbol{x}) = \mathbf{P}^T(\boldsymbol{x})\mathbf{a}(\boldsymbol{x}) = \sum_{i=1}^{m} P_i(\boldsymbol{x}) a_i(\boldsymbol{x}) \tag{1}$$

where *m* denotes the number of terms in the basis. In two dimensions a complete polynomial basis of order m is given by

$$\mathbf{P}^T(x,y) = \left(1, x, y, x^2, xy, y^2, ..., x^m, ..., x^m y^{m-k}, ..., y^m\right) \tag{2}$$

For bi-linear, the basis function is considered as

$$\mathbf{P}^T(x,y) = (1, x, y, xy),\ m=4 \tag{3}$$

Also, the linear basis is provided by

$$\mathbf{P}^T(x,y)=(1,x,y),\ m=3 \tag{4}$$

Vector of unknown parameters that depended on x is given as

$$\mathbf{a}(\boldsymbol{x})=(a1(x),a2(x),...,a_m(x)) \tag{5}$$

These basis functions are not required to be polynomials as shown in Equations 3 and 4. When solving problem involving cracks, a convenient way of capturing $1/\sqrt{r}$ stress-singularity in linear-elastic fracture mechanics is calculated by using [19,20]

$$\mathbf{P}^T(x,y)=\left(1,x,y,\sqrt{r}\right),\ m=4 \tag{6}$$

Or

$$\mathbf{P}^T(x,y)=\left(1,x,y,\sqrt{r}\cos\left(\theta/2\right),\sqrt{r}\sin\left(\theta/2\right),\sqrt{r}\sin(\theta/2)\sin\theta,\sqrt{r}\cos\left(\theta/2\right)\sin\theta\right),m=7 \tag{7}$$

Where r and θ are polar coordinates with the crack tip as the origin. Equations 6 and 7 represent fully enriched and partially enriched basis functions, respectively.

In the equations 1, the coefficient vector, $\mathbf{a}(x)$ is determined by minimizing a weighted discrete L_2 norm, defined as

$$J(\boldsymbol{x})=\sum_{I=1}^{n}w(\boldsymbol{x}-\boldsymbol{x}_I)\left(\mathbf{P}^T(\boldsymbol{x}_I)\mathbf{a}(\boldsymbol{x})-u_I\right)^2 \tag{8}$$

Where n is the number of nodes I such that $w(x-x_I)\succ 0$; $w_I(x)=w(x-x_I)$ is the weight function associated with node I which is non-zero over a limited support called the influence domain of node I. Furthermore, it is assumed that $w_I(x)$ is non-increasing for $0\le d\le d_{mI}$, where $d=\|x_I-x\|$. The parameter d_{mI} determines the influence domain of node I for weight functions. Equation 8 can also be written as [15]

$$J(\boldsymbol{x})=(\mathbf{Pa}(\boldsymbol{x})-\mathbf{u})^T\mathbf{W}(\mathbf{Pa}(\boldsymbol{x})-\mathbf{u}) \tag{9}$$

Where

$$\mathbf{u}^T=(u_1,u_2,...,u_n) \tag{10}$$

$$\mathbf{P}=(\mathbf{P_{ij}})_{n\times m}=\begin{bmatrix}1 & x_1 & y_1 & x_1y_1\\ 1 & x_2 & y_2 & x_2y_2\\ \vdots & \vdots & \vdots & \vdots\\ 1 & x_n & y_n & x_ny_n\end{bmatrix} \tag{11}$$

$$\mathbf{W}(\boldsymbol{x}) = \left(w_{ij}\right)_{n\times n} = \begin{bmatrix} w(\boldsymbol{x}-\boldsymbol{x}_1) & 0 & \cdots & 0 \\ 0 & w(\boldsymbol{x}-\boldsymbol{x}_2) & \cdots & 0 \\ \vdots & & \ddots & \\ 0 & 0 & \cdots & w(\boldsymbol{x}-\boldsymbol{x}_n) \end{bmatrix} \tag{12}$$

The stationarity of $J(\boldsymbol{x})$ with respect to $\boldsymbol{a}(\boldsymbol{x})$ yields

$$\frac{\partial J}{\partial \mathbf{a}} = \mathbf{A}(\boldsymbol{x})\mathbf{a}(\boldsymbol{x}) - \mathbf{B}(\boldsymbol{x})\mathbf{u} = 0 \tag{13}$$

Therefore,

$$\mathbf{B}(\boldsymbol{x}) = \mathbf{P}^T\mathbf{W}(\boldsymbol{x}) \tag{15}$$

$$= \left[w(\boldsymbol{x}-\boldsymbol{x}_1)\mathbf{P}(\boldsymbol{x}_1) \quad w(\boldsymbol{x}-\boldsymbol{x}_2)\mathbf{P}(\boldsymbol{x}_2) \quad \cdots \quad w(\boldsymbol{x}-\boldsymbol{x}_n)\mathbf{P}(\boldsymbol{x}_n)\right]$$

The MLS approximants can be defined as

$$u^h(\boldsymbol{x}) = \sum_{I=1}^{n} \boldsymbol{\phi}_I(\boldsymbol{x})u_I = \boldsymbol{\Phi}(\boldsymbol{x})\mathbf{u} \tag{16}$$

Where the shape function $\boldsymbol{\Phi}_I(\boldsymbol{x})$ is

$$\boldsymbol{\Phi}_I(\boldsymbol{x}) = \mathbf{P}^T(\boldsymbol{x})\mathbf{A}^{-1}(\boldsymbol{x})\mathbf{B}_I(\boldsymbol{x}) \tag{17}$$

The partial derivatives of $\boldsymbol{\Phi}_I(\boldsymbol{x})$ can be obtained as follows

$$\boldsymbol{\Phi}_{I,i}(\boldsymbol{x}) = \sum_{j=1}^{m} \left\{ p_{j,i}\left(\mathbf{A}^{-1}\mathbf{B}\right)_{jI} + p_j\left(\mathbf{A}_{,i}^{-1}\mathbf{B} + \mathbf{A}^{-1}\mathbf{B}_{,i}\right)_{jI} \right\} \tag{18}$$

In which $(\ )_{,i} = \dfrac{\partial(\ )}{\partial x_i}$.

THE EFG FORMULATION

Consider a two dimensional problem. By substituting the approximation in Equation 16 into the associated Galerkin weak form, one can obtain the final form of the discredited system of equations [2,15,20]

$$\begin{bmatrix} \mathbf{K} & \mathbf{G} \\ \mathbf{G}^T & 0 \end{bmatrix} \begin{Bmatrix} \mathbf{u} \\ \boldsymbol{\lambda} \end{Bmatrix} = \begin{Bmatrix} \mathbf{f} \\ \mathbf{q} \end{Bmatrix} \tag{19}$$

Where

$$\mathbf{K}_{ij} = \int_{\Omega} \mathbf{B}_i^T \mathbf{D} \mathbf{B}_j d\Omega \tag{20}$$

$$\mathbf{G}_{ik} = -\int_{\Gamma u} \mathbf{\Phi}_i \mathbf{N}_k d\Gamma \tag{21}$$

$$\mathbf{f}_i = \int_{\Gamma t} \mathbf{\Phi}_i \bar{\mathbf{t}} d\Gamma + \int_{\Omega} \mathbf{\Phi}_i \mathbf{b} d\Omega \tag{22}$$

$$\mathbf{q}_k = -\int_{\Gamma u} \mathbf{N}_k \bar{\mathbf{u}} d\Gamma \tag{23}$$

Where $\bar{\mathbf{t}}, \mathbf{b}, \mathbf{D}$ and $\boldsymbol{\lambda}$ are specified traction vector, body force vector, matrix of elastic constants and vector of Lagrange multipliers, respectively. Matrices $\mathbf{B}, \mathbf{\Phi}$ and $\mathbf{N}$ are defined as follows

$$\mathbf{B}_i = \begin{bmatrix} \phi_{i,x} & 0 \\ 0 & \phi_{i,y} \\ \phi_{i,y} & \phi_{i,x} \end{bmatrix} \tag{24}$$

$$\mathbf{\Phi}_i = \begin{bmatrix} \phi_i & 0 \\ 0 & \phi_i \end{bmatrix} \tag{25}$$

$$\mathbf{N}_k = \begin{bmatrix} N_k & 0 \\ 0 & N_k \end{bmatrix} \tag{26}$$

In Equation (26), $\mathbf{N}_k$ are the conventional FEM shape functions which are used for the approximation of Lagrange multipliers on the essentials boundaries [4, 15]. This is because as mention, the MLS shape functions do not possess the Kronecker delta function property.

In the process of generation of the system of Equation (19), two domain integrals must be computed. These integrals are involved in the stiffness matrix, Equation (20), and load vector Equation (22). Usually in the EFG method, these two integrals are computed by Gaussian quadrature method [19].

THE INFLUENCE OF DOMAIN FORM

The shape functions $\mathbf{\Phi}_i$ are obtained from the weight functions, these functions have influence domain of the node. The domain size is defined by the so called dilatation parameter or smoothing length. It is critical to solution accuracy, stability and plays the role of the element size in the finite element method. The final characteristics of weight functions are its functional forms. The weight function should be continuous and positive in its support. Some commonly used weight functions are

• the cubic spline weight function:

$$w(r)=\begin{cases}\frac{2}{3}-4r^2+4r^3, & r\le\frac{1}{2}\\ \frac{4}{3}-4r+4r^2-\frac{4}{3}r^3, & \frac{1}{2}\prec r\le 1\\ 0, & r\succ 1\end{cases} \tag{27}$$

• The quadratic spline weight function:

$$w(r)=\begin{cases}1-6r^2+8r^3-3r^4, & r\le 1\\ 0, & r\succ 1\end{cases} \tag{28}$$

With

$$r=\frac{d}{d_{mI}} \tag{29}$$

Where r is the normalized distance between the node **I** and point **x**.

The parameter d_{mI} for each node should be chosen large enough that matrix **A** be invertible everywhere in the domain. Also, it should be small enough to retain the local characteristic of the approximation. Equation 29 directly applicable in a circular domain as in the following equation:

• Two dimensions, circular domain

$$w(\mathbf{x}-\mathbf{x_I})=w\left(\frac{\|\mathbf{x_I}-\mathbf{x}\|}{d_{mI}}\right) \tag{30}$$

In elliptic weight functions, each node has a major radius of influence d_{mIx}, a minor radius of influence d_{mIy} and an angle θ that determines the direction of the maximum radius of the influence ellipse. The influence elliptic domain of a node is determined by three parameters in contrast to one in the circular domain weights. The availability of more controlling parameters for determination of the influence domain of each node helps to increase computational efficiency of EFGM. The normalized distance in the elliptic form (2D) is

$$r=\sqrt{\left(\frac{\mathbf{x}-\mathbf{x_I}}{d_{mIx}}\right)^2+\left(\frac{\mathbf{y}-\mathbf{y_I}}{d_{mIy}}\right)^2} \tag{31}$$

The use of the circular support may add the number of points in the influence domain of a node ineffectively. In the Figure 2, the influence domain or support of a node that is at the center of the ellipse or circle is shown. There are more sample points such as integration points in the circular support than the elliptic support.

The derivatives of the weight functions can be computed using the chain rule. For example, for circular supports:

$$w_k(r) = w_r(r) r_k = w_r \frac{x_k - x_{Ik}}{rd_{mI}^2} \tag{32}$$

NUMERICAL RESULTS

Example 1. The performance of elliptic domain is studied for Timoshenko beam (Figure 3). The problem is solved for P =1000 as a parabolic tangential stress at the free end, $E = 3.0 \times 10^7$, and v = 0.3. The beam is considered to be of unit depth and it is in plane stress state. This problem was numerically solved by [4, 15, 20].

The regular node distribution together with the background mesh that is used for numerical integration of the weak form is shown in Figure 4. In each integration cell, 4 × 4 Gauss quadrature is used. A linear basis and cubic spline weight function are used in the MLS approximation. For this problem, circular nodal support of radius 3.5 times from longer nodal spacing is employed ($d_{mI} = 3.5 \times longer - nodal - spacing$). Also, elliptical nodal support of radius 3.5 times from longer nodal spacing ($d_{mIx} = 3.5 \times longer - nodal - spacing$), and smaller nodal spacing ($d_{mIy} = 3.5 \times smaller - nodal - spacing$), in x and y direction respectively are employed.

In Table 1, the vertical displacement at the point (L,0) calculated by EFG is compared with the exact solution. This table shows excellent agreement between EFG and the analytical solution, particularly in the results of the elliptic domain. For more clarification, the deflection of the beam is shown in Figure 5. Also, The stresses at the center of the beam (x = L/2, y∈[−D/2,D/2]) compared with the exact solution are shown in Figure 6. In addition, the distribution of the stresses in the beam is plotted in Figure 7. It is of particular interest that very smooth stresses are obtained by using the elliptic domain-EFGM without any additional treatment as is necessary in FEM.

Furthermore, reduction of computational cost is verified. The ratio of the elapsed time for solving the problem with elliptic domain to the circular domain is approximately equal to 0.61 at 1800 field nodes. This is due to less value of n in Equation 8 when the elliptic domain is used.

Example 2. This example involves cracked plate under remote tension (Figure 8). Consider an infinite plate in stretching with crack at the center. Due to the symmetry, twofold symmetry (ABCD) is used as a model for this problem. Along ABCD the closed form solution in terms of polar coordinates in a reference frame (r,θ) centered at the crack tip is

$$u_x(r,\theta) = \frac{2(1+\nu)}{\sqrt{2\pi}} \frac{K_I}{E} \sqrt{r} \cos\frac{\theta}{2}\left(2 - 2\nu - \cos^2\frac{\theta}{2}\right) \tag{33}$$

$$u_y(r,\theta) = \frac{2(1+\nu)}{\sqrt{2\pi}} \frac{K_I}{E} \sqrt{r} \sin\frac{\theta}{2}\left(2 - 2\nu - \cos^2\frac{\theta}{2}\right) \tag{34}$$

Where K_I is the stress intensity factor, υ is Poisson's ratio and E is Young's modulus. The square of 10mm×10mm, a=100 mm; $E = 10^3$ N/mm^2, $\upsilon = 0.3$ and remote stress of unit N/mm^2.

Enriched EFGM is used to solve this example where the re-mesh (redistribute of nodes in the crack tip region) is not needed. Geometry of the crack is created as a line as shown in Figure 9 by using the level set method [20]. Additionally, same figure shows the detection of the enriched method for the nodes with the elliptic domains set. More information about the enriched meshless method is found in [9]. After the solution, the error of the displacement norm by using the circular

and the elliptic domain is extracted. Table 2 is cleared that the results by using elliptic support is better than using circle support.

Anyway, major advantages of the use elliptic support in the cracked plate problem can be demonstrated in the following points:

1. The error of the displacement norm is curtailed, and it is decreased rapidly when the nodes increase or when the area of the elliptic decrease. This gives the problem multi other parameters to control on the numerical solution.

2. Reduction of computational cost is occurred. This is due to less value of the nodes in the local domain (support).

3. The reach path to the final solution is done under a small total number of nodes. This can be illustrated by Figure 10-12 that done at same longer domain size. Figure 10 represents the exact distribution of stress σ_{yy}, that is more coincide with Figure 11, which represents the distribution of numerical stress σ_{yy} using the elliptic domain. It is a very clear the failure of the distribution of numerical stress using the circle domain for the exact distribution, as in Figure12.

CONCLUTIONS

Elliptic domain of influence is used in the element free Galerkin method to study the possibility of using this local domain in the computational mechanics. This domain changes the behavior of work of the used weight function in the extract the data from the nodes, because in the elliptic support, each node has three characteristic indications that are major radius, inner radius, and the direction of major local domain .

Furthermore, the space that is covered by the elliptic domain is less than the area of the circle domain at the same main diameter, and this reduces the computational time of the required calculation. Also, the smooth final solution is done under a small total number of nodes reverse as happens in traditional domain. Thus, using this domain, influence domain of a node is determined by three parameters in contrast to one in the other domains. The availability of more controlling parameters for determination of the influence domain of each node helps to increase computational efficiency of EFGM. This paper can be extended by changing the direction of major local domain in the calculation, as well as in the use of the domain in the other advanced applications.

REFERENCES

[1] P. Lancaster and K. Salkauskas "Surfaces Generated by Moving Least Squares Methods", Mathematics of Computation, Vol. 37, pp. 141-158, 1981

[2] T. Belytschko, Y. Y. Lu, and L., Gu, "Element-Free Galerkin Methods", International Journal for Numerical Methods in Engineering, Vol. 37, pp. 229-256, 1994.

[3] Y. Y. Lu, T. Belytschko, and, L. Gu, "A New Implementation of the Element Free Galerkin Method", Computer Methods in Applied Mechanics and Engineering, Volume 113, Pages 397-414, 1994.

[4] J. Dolbow, and T. Belytschko, "An Introduction to Programming the Meshless Element Free Galerkin Method", Achieves of Computational Mechanics, Vol.15, No. 3, pp. 207-241, 1998.

[5] T. Belytschko, Y. Krongauz, M. Fleming, D. Organ, W. Liu "Smoothing and Accelerated Computations in the Element Free Galerkin Method", J. of Computational and Applied Mathematics, Vol. 74, pp. 111–126, 1996.

[6] T. Belytschko, Y.Y. Lu, "Element-Free Galerkin Methods for Static and Dynamic Fracture", Int. J. Solids Struct. 32 (1995) 2547–2570.

[7] T. Belytschko, Y.Y. Lu, L. Gu, "Crack Propagation by Element-Free Galerkin Methods", Eng. Fract. Mech. 51 (2) (1995) 295–315.

[8] T. Belytschko, L. Gu,Y.Y. Lu, "Fracture and Crack Growth by Element-Free Galerkin Methods", Model. Simul. Mater. Sci. Eng. 2 (1994) 519–534.

[9] S. Bordas, T. Rabczuk, and G. Zi, "Three-Dimensional Crack Initiation, Propagation, Branching and Junction in Non-Linear Materials by Extrinsic Discontinuous Enrichment of Meshfree Methods Without Asymptotic Enrichment". Eng Fract Mech. 75 (2008) 943–960.

[10] T. Rabczuk, T. Belytschko, "Cracking Particles: a Simplified Meshfree Method for Arbitrary Evolving Cracks". Int J Numer Methods Eng. 61 (13) (2004) 2316–2343

[11] T. Rabczuk, P.M.A. Areias, T. Belytschko, "A Simplified Meshfree Methods for Shear Bands with Cohesive Surfaces", Int. J. Numer. Methods Eng. 69 (5) (2007) 993–1021.

[12] S. Li, W. Hao, W.K. Liu, "Meshfree Simulations Shear Banding Under Large Deformation". International Journal of Solids and Structures 37, (2000) 7185–7206.

[13] W. Shouxin, "Computational Simulation of Strain Localization: From Theory to Implementation", MSc Thesis, College of Engineering and Science Louisiana Tech University, 2009.

[14] T. Rabczuk, P. M. A. Areias, and T. Belytschko, "A Simplified Mesh-Free Method for Shear Bands with Cohesive Surfaces", Int. J. Numer. Meth. Engng 69 (2007) 993–1021.

[15] G.R. Liu., "Meshfree Methods-Moving Beyond the Finite Element Method", Book, Taylor and Francis Group, LLC, (2010)

[16] Y. Krongauz, and T. Belytschko, "Enforcement of Essential Boundary Conditions in Meshless Approximations Using Finite Elements", Comput. Methods Appl. Mech. Eng., 131(1–2) (1996) 133–145.

[17] G. R. Liu, M. B Liu, and K. Y. Lam, , "A General Approach for Constructing Smoothing Functions for Meshfree Methods", Presented at Ninth International Conference on Computing in Civil and Building Engineering, Taipei, China, April 3–5, (2002) 431–436.

[18] G.R. Liu, "An Introduction to the Programming of Meshfree Methods", Book, Springer, (2005)

[19] B. N. Rao, and A. S. Balu., "Fuzzy Meshfree Method for Fracture Analysis of Cracks"، ASME Pressure Vessels and Piping Division Conference, (2007) PVP2007-26792.

[20] V. P. Nguyena, T. Rabczuk, S. Bordas, and M. Duflot, "Meshless Methods: A Review and Computer Implementation Aspects", Math. and Comp. in Simulation 79 (2008) 763–813.

Table(1): Comparsion of Vertical Displacement End of Beam

Nodes	u_y Exact	u_y EFGM		Error %	
		Elliptic Domain	Circular Domain	Elliptic Domain	Circular Domain
7 x 5	-0.00890	-0.00848	-0.00831	-4.71	-6.26
11 x 5	-0.00890	-0.00877	-0.00868	-1.46	-2.47
15 x 9	-0.00890	-0.00881	-0.00879	-1.01	-1.23
20 x 9	-0.00890	-0.00881	-0.00879	-1.00	-1.23
30 x 15	-0.00890	-0.00883	-0.00882	-0.78	-0.89
60 x 30	-0.00890	-0.00890	-0.00884	0.00	-0.67

Table(2): The Error of the Displacement Norm Results

Nodes	Circular Domain Size d_{mI}	Disp. Norm Error	Elliptic Domain Size $d_{mIx} \, x \, d_{mIy}$	Disp. Norm Error
5 x 5	2.5	0.372	2.5 x 2.25	0.372
			2.5 x 2.00	0.362
			2.5 x 1.50	0.202
7 x 7	2.5	0.115	2.5 x 2.25	0.103
			2.5 x 2.00	0.102
			2.5 x 1.50	0.075
10 x 10	2.5	0.081	2.5 x 2.25	0.073
			2.5 x 2.00	0.043
			2.5 x 1.50	0.028

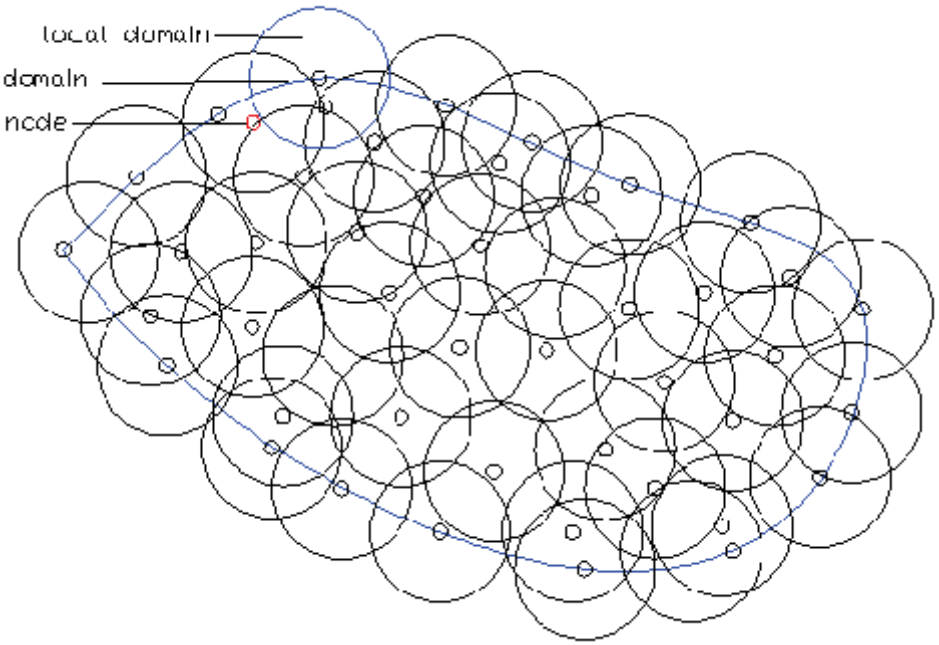

Fig. (1) Discretization Using Meshless Methods - Nodes, Circular Domains of Influence.

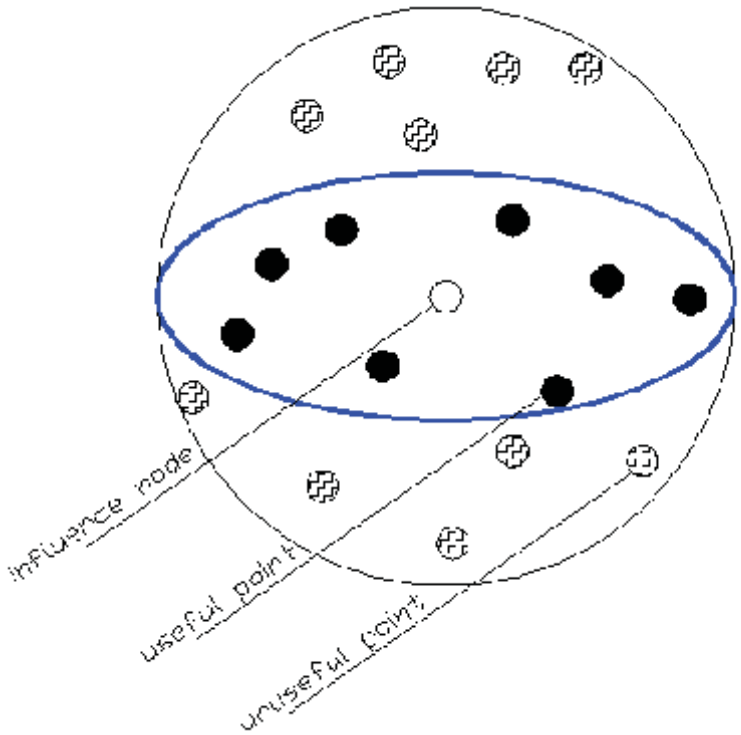

Fig. (2) Requirement Representation of Elliptic Domain, and Circular Domain to the Integrations Points.

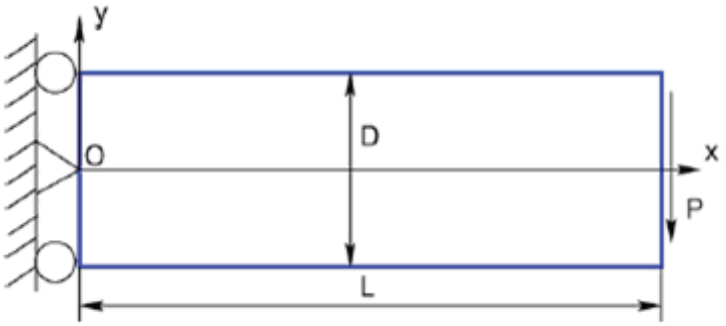

Fig. (3) The Timoshenko Beam.

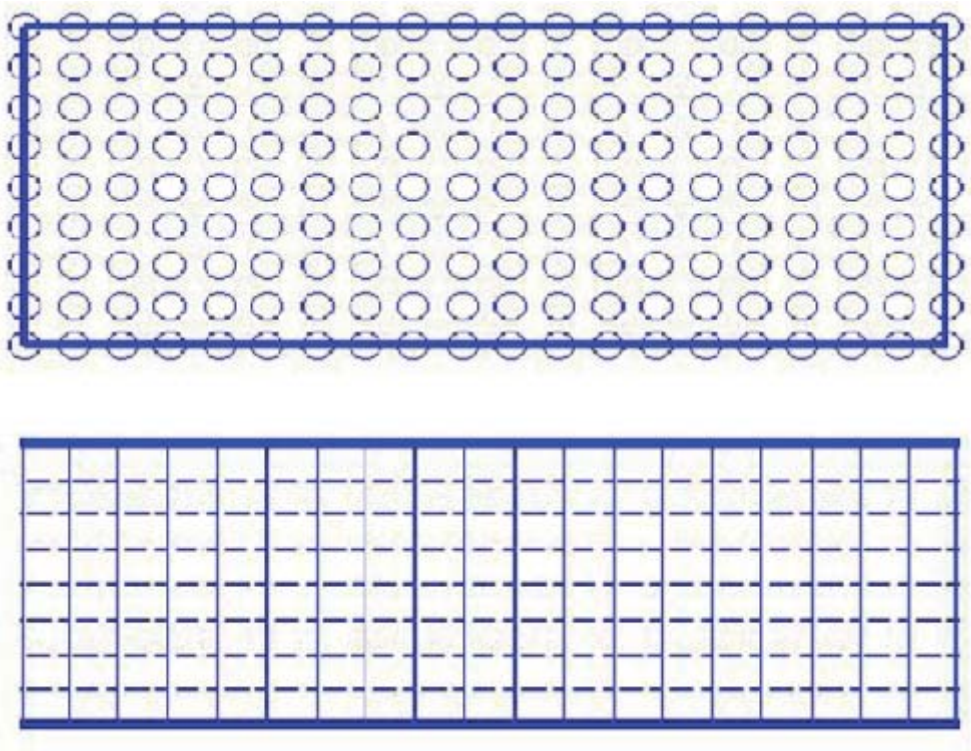

Fig. (4) 20 x 9 Regular Nodes Distribution with Background Mesh Configuration for the Timoshenko Beam.

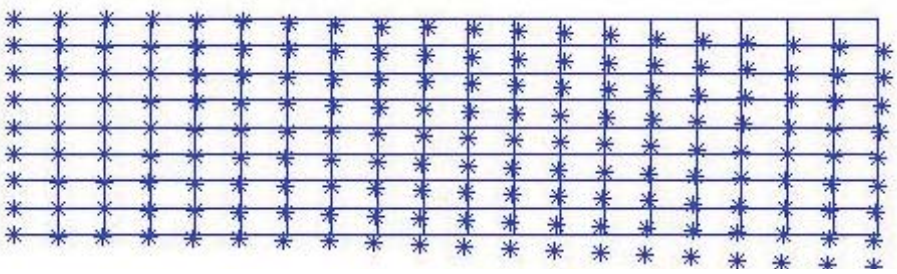

Fig. (5) Deflection Representation of the Beam.

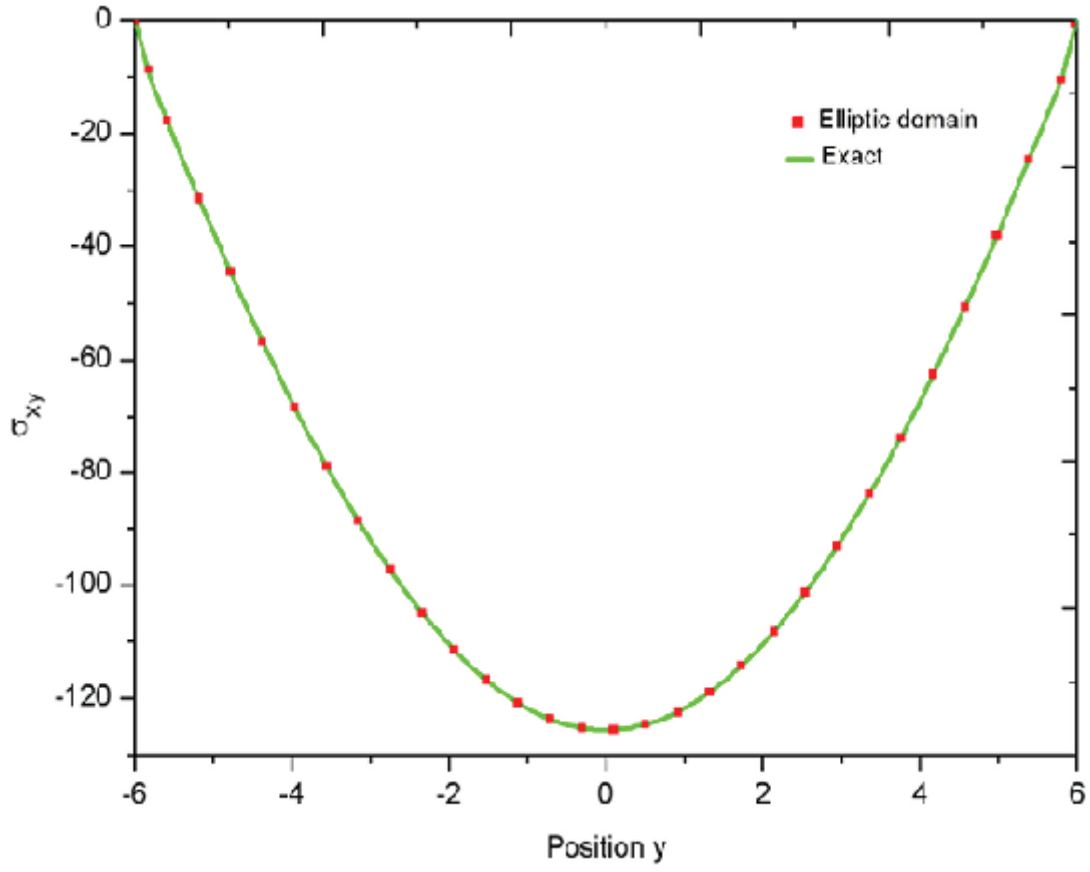

Fig. (6/a) Stress Comparison, Shear Stress.

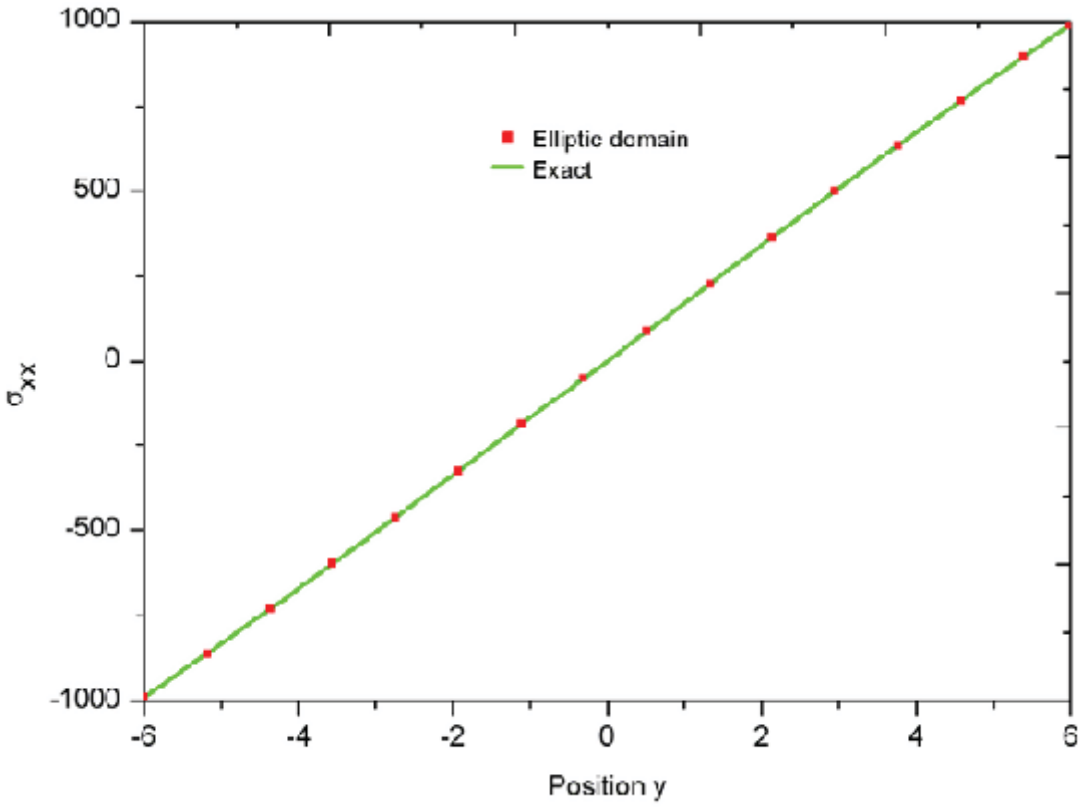

Fig. (6/b) Stress Comparison, Normal Stress.

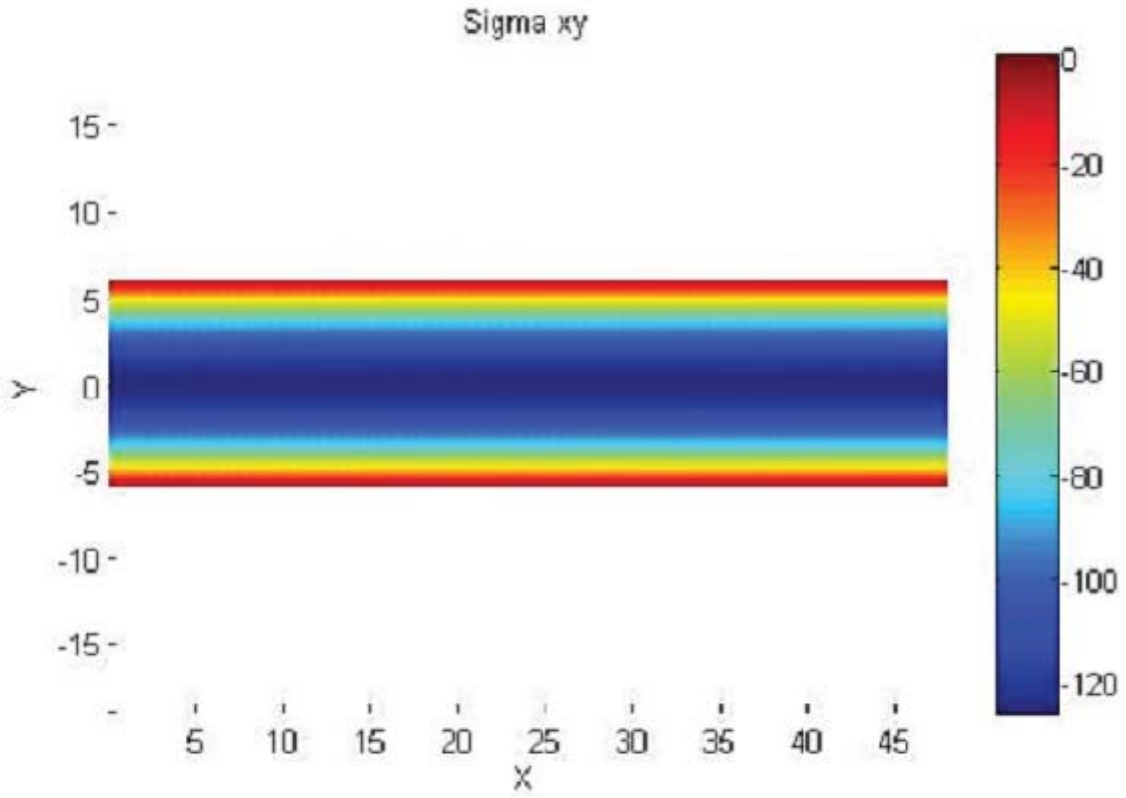

Fig. (7/a) Stress Distribution, Shear Stress σ_{xy}.

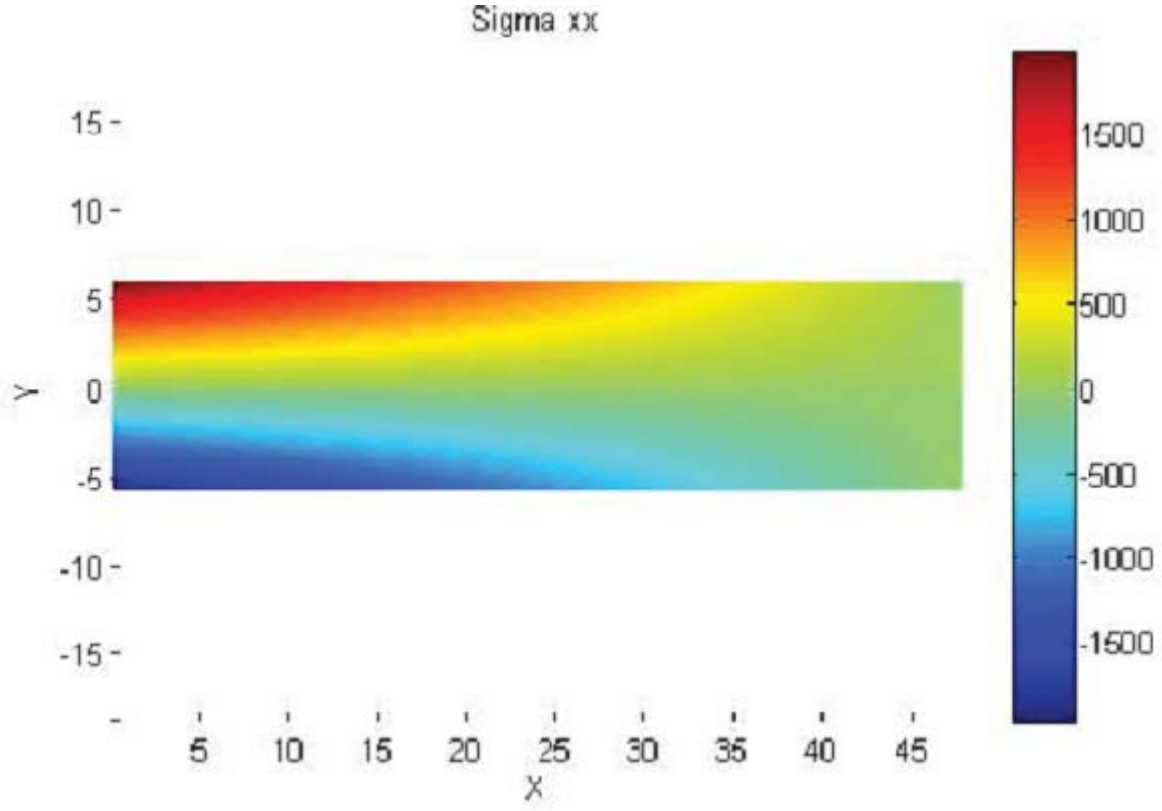

Fig. (7/b) Stress Distribution, Normal Stress σ_{xx}.

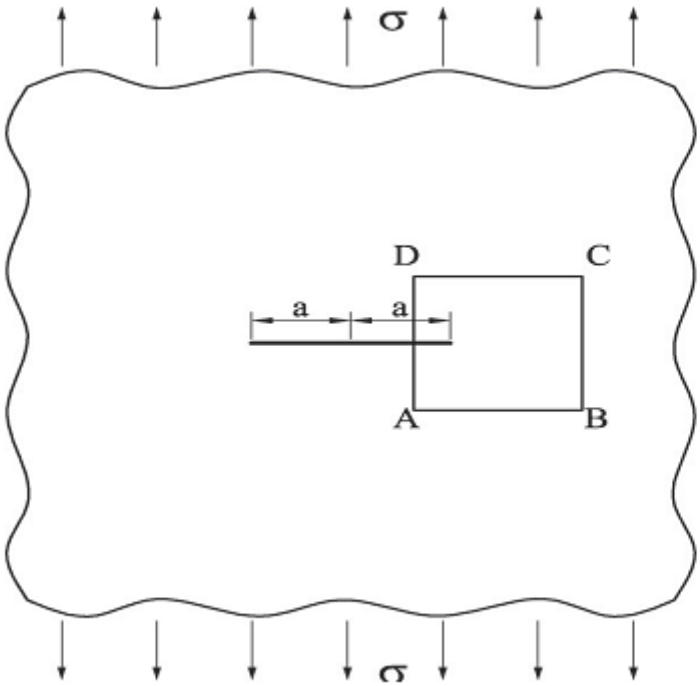

Fig. (8) Infinite Cracked Plate Under Remote Tension.

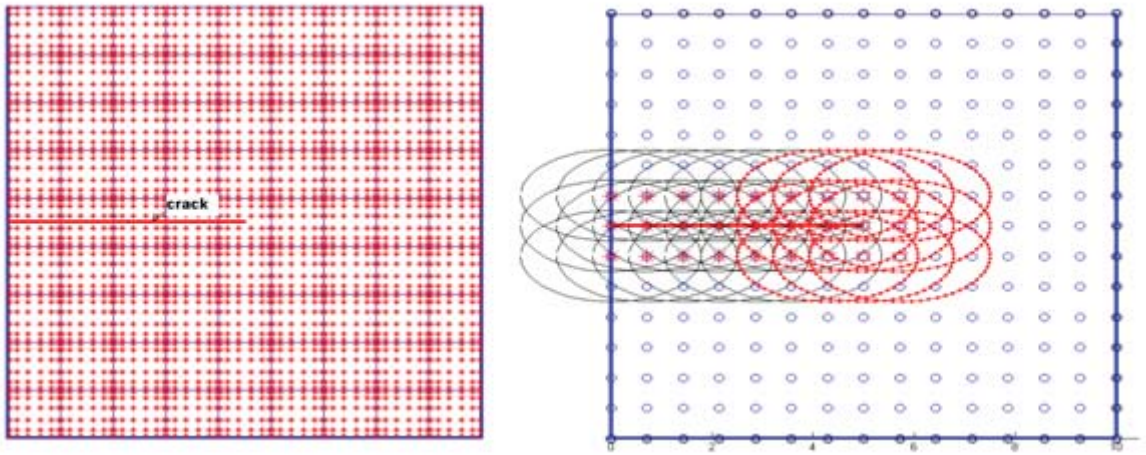

Fig. (9) Creation and Detection of ABCD Crack.

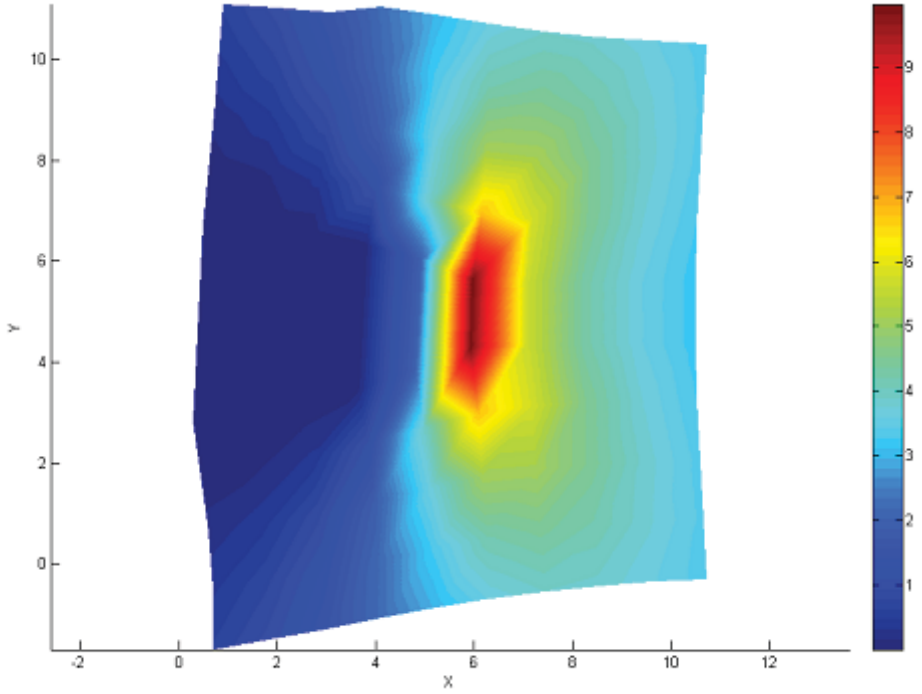

Fig. (10) Exact Stress Distribution (Deformed Scaled).

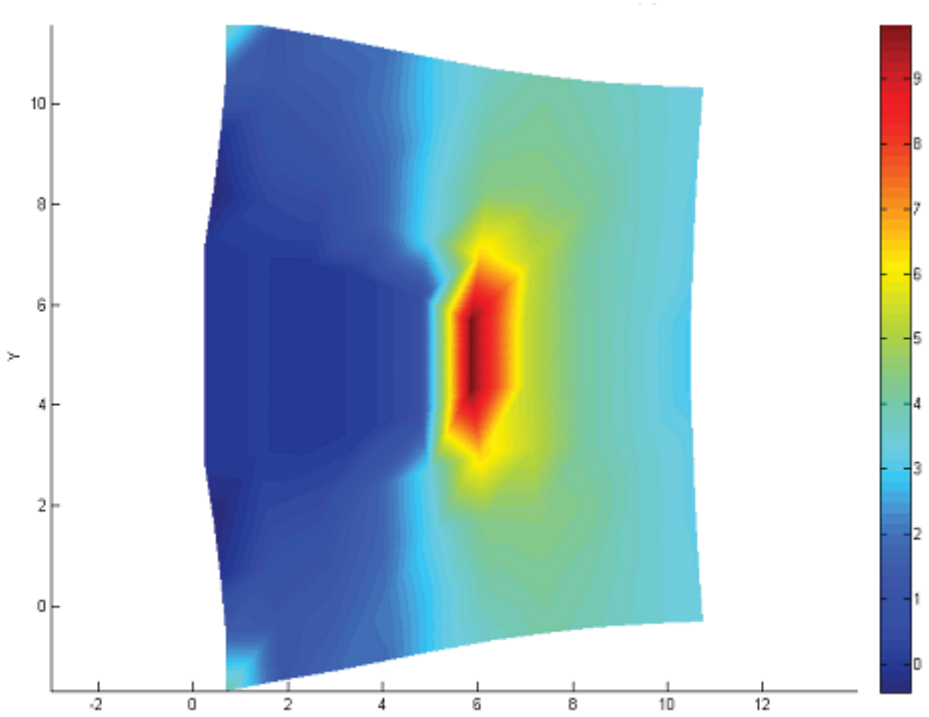

Fig. (11) Numerical (Elliptic Domain Used) - Stress Distribution (Deformed Scaled).

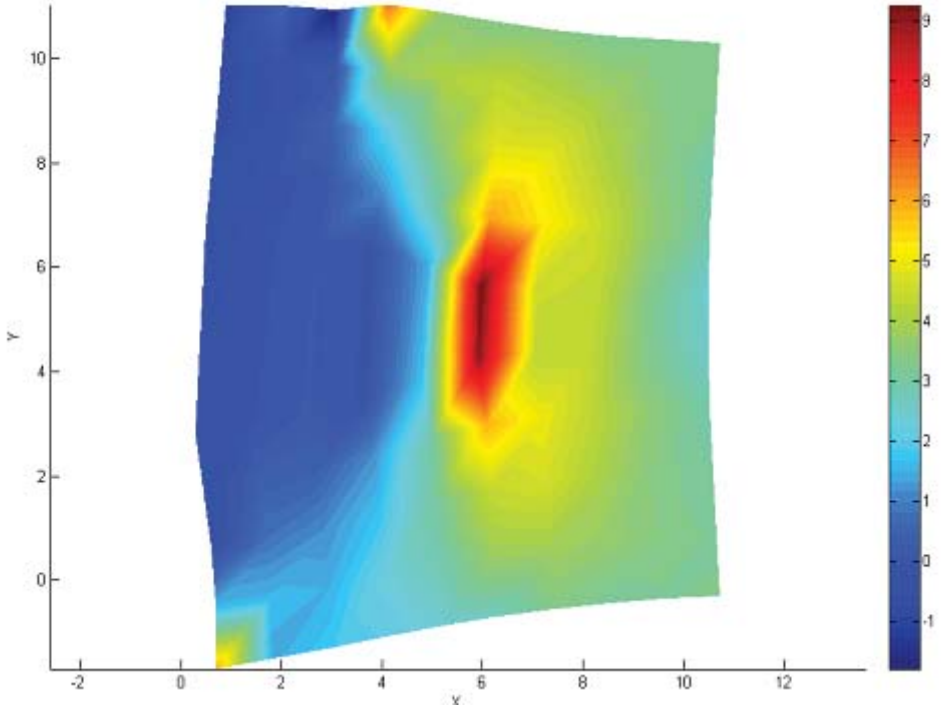

Fig. (12) Numerical (Circle Domain Used) - Stress Distribution (Deformed Scaled).